Science

AAAS

Seismic Anisotropy: Tracing Plate Dynamics in the Mantle

Seismic Anisotropy: Tracing Plate Dynamics in the Mantle

Jeffrey Park and Vadim Levin

Elastic anisotropy is present where the speed of a seismic wave depends on its direction. In Earth's mantle, elastic anisotropy is induced by minerals that are preferentially oriented in a directional flow or deformation. Earthquakes generate two seismic wave types: compressional (*P*) and shear (*S*) waves, whose coupling in anisotropic rocks leads to scattering, birefringence, and waves with hybrid polarizations. This varied behavior is helping geophysicists explore rock textures within Earth's mantle and crust, map present-day upper-mantle convection, and study the formation of lithospheric plates and the accretion of continents in Earth history.

The rocks of Earth's upper mantle deform in the slow convective flows of our planet's hot interior. Deformation preferentially aligns mineral crystals within rock (*1–3*). This alignment induces elastic anisotropy, which affects how fast seismic waves propagate in different directions. In principle, measurement of wavespeed directionality and related seismic properties can image deformation in the rocks of Earth's mantle and may illuminate the mantle's role in plate motion. Seismic indicators of anisotropy are often subtle and can have conflicting interpretations. A simple image of Earth's present-day mantle flow is complicated by several factors, including textures produced in past deformation episodes, total strain, shear style, temperature, and volatile content, all of which influence microscopic processes within deforming mineral crystals (*4–9*).

Here we review recent studies of upper-mantle anisotropy and its relation to global plate motions, past and present. Four basic seismic wave behaviors have been used to identify seismic anisotropy: direction-dependent travel time anomalies, shear-wave birefringence, surface-wave scattering, and direction-dependent conversion of compressional (*P*) to shear (*S*) waves. Each approach has advantages and disadvantages.

Mechanisms for Developing Anisotropy

Anisotropy is found on several scales. Many rocks are anisotropic on the scale of individual minerals (*4*, *5*), or have a preferred alignment of microcracks or pore spaces (*10*). Larger scale geologic textures can also produce seismic anisotropy, as when different rock types are interlayered on scales much

Department of Geology and Geophysics, Yale University, Post Office Box 208109, New Haven, CT 06520–8109, USA.

smaller than the wavelengths of seismic *P* and *S* waves (*11*) (>500 m for typical earthquake signals). Crack-induced and fine-layering anisotropy are most prevalent in the uppermost crust, but the effects of macroscopic rock texture may be important in some of the mantle near the base of the crust (*12*, *13*). A sequence of veins from the ascent of basalt or fluids through the lithosphere can also produce seismic anisotropy (*14*).

The mineral olivine makes up 40% or more of typical mantle rock (such as peridotite) shallower than 420 km depth. The stiffness of olivine varies substantially among its three different crystallographic axes, so that seismic wavespeed in a single crystal varies with direction by 20 to 25% (*2*). Only a modest alignment in olivine is necessary to generate anisotropies of 2 to 6% (*8*), which are commonly observed. Mantle flow orients minerals by producing slip on vulnerable glide planes within the crystal lattice. However, laboratory experiments confirm that for olivine the slip planes cannot accomodate all crystal deformations required by continuum theory, so that many grains harden as strain proceeds. Other deformation mechanisms may then become important, caused by crystal breakage, subgrain rotation, diffusion, or the absorption of highly deformed crystals into less deformed neighbors via grain-boundary migration (*15*, *16*). These forms of recrystallization tend to alter and erase earlier fabrics.

Encouraged by studies of ophiolites (*5*), seismologists often assume that the two slower olivine crystal axes scatter randomly perpendicular to the average fast axis, so that strained mantle rock would have hexagonal symmetry, with a fast axis aligned with maximum extension. Early continuum and quasi-continuum theories confirmed that the fast compressional wavespeeds (V_P) of olivine would align with the direction of maximum

extension in simple shear (Fig. 1) or the plane of extension in axial compression (*8*, *17*). Media with hexagonal symmetry can be described by three anisotropic parameters (*18*), but only two find common usage in global seismology, one each for V_P and V_S anisotropy. The symmetry axis can be fast, as for strained olivine-rich rock (*6*), or slow, as for anisotropy induced by cracks and/or fine-layered isotropic media (*10*, *11*). If the symmetry axis is vertical, anisotropy affects mainly wavespeeds. Horizontal and plunging symmetry axes induce polarization birefringence and amplify scattering between wave types.

Laboratory experiments can be used to predict anisotropic scenarios in the upper mantle, though all likely factors remain to be tested. Zhang and Karato (*6*) found that the fast axis follows principal extension in modestly deformed olivine aggregates (<100% strain) but aligns with the direction of flow for large deformations (Fig. 1). This result suggests that modest simple shear, such as may occur at the base of a moving plate, will produce anisotropy with a plunging axis of symmetry. Modest pure shear in the horizontal plane, associated with rifting extension or orogenic compression, would align the symmetry axis with the flow direction. Accumulated simple-shear flow from thermal convection would also align the symmetry axis with the flow direction. The presence of water can alter the relative strengths of olivine slip planes and change how it deforms (*9*). Thus, interpreting seismic anisotropy in regions of abundant volatiles, such as in the supraslab mantle wedge of island-arc subduction zones, may be complicated.

Anisotropy from Phase-Delay Tomography

The first confirmations of seismic anisotropy in the uppermost mantle came from the directional wavespeed variation of *P* waves that travel along the crust-mantle interface, the so-called P_n phase (*18*, *19*). Direction-dependent wavespeed variations in *P*, *S*, and surface waves can be localized with seismic tomography, which compares phase delays of intersecting wavepaths from a broad distribution of sources and receivers. Most tomographic models of Earth elasticity do not include seismic anisotropy. The simplest anisotropic models
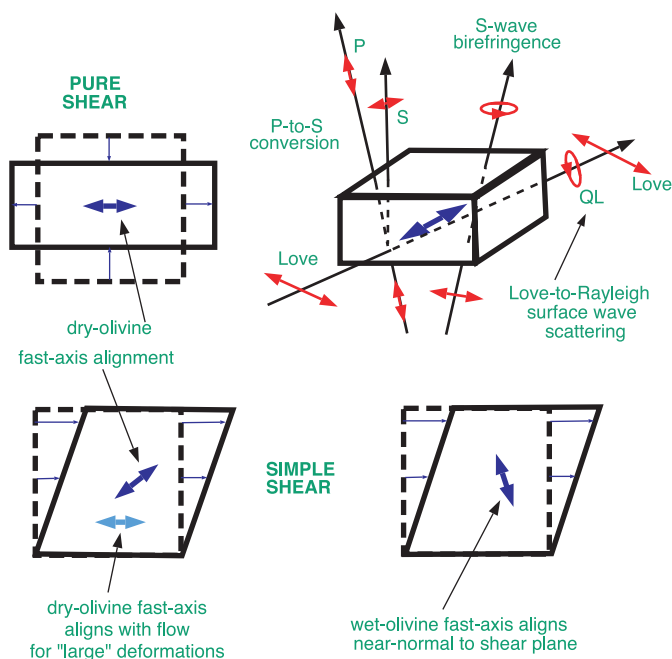
Fig. 1. Predicted alignment of the olivine fast axis in mantle deformations, based on high-pressure shear experiments (*6*, *9*, *15*). Wet olivine corresponds to a concentration of >600 parts per million H/Si, shear stress σ < 325 MPa, confining pressure $P \approx 2$ GPa, and 1400°< T < 1570°K (where T is temperature) (*9*). The image at upper right illustrates birefringence and scattering effects caused by elastic anisotropy. Red arrows indicate rectilinear wave polarization. Red ellipses indicate elliptical wave polarization.

use Rayleigh and Love surface waves as data and include a 50- to 200-km-thick upper mantle layer that is 1 to 3% anisotropic with a slow vertical axis of symmetry (*20*). This could be the effect of fine horizontal layering in the shallow mantle; dense raypath coverage in the Pacific Ocean region argues against the averaged effect of a horizontal fast axis on a global distribution of surface-wave propagation paths (*21*). Long-period surface waves exhibit a directional dependence as well, which requires a horizontal or plunging axis of symmetry (*22*). Anisotropy tends to be modest in global models (1 to 3%) and can largely be confined to the upper 200 km of the mantle under oceanic plates (*23*, *24*). This suggests that shear textures associated with moving plates do not extend deeply into the asthenosphere.

Geographic variations in anisotropy (Fig. 2) tend to explain a small proportion of data variance in global surface-wave tomographic inversions and are difficult to distinguish from short-wavelength isotropic V_P and V_S anomalies (*25–28*). An interpretation in terms of anisotropy is bolstered by the strong correlation of inferred fast axes with spreading direction along the Pacific and Indian Ocean ridge systems (*23*, *25–27*) and the Atlantic ridge between 0° and 45°N (*29*). Correlation with plate motion is less straightforward for other plate boundary types, owing perhaps to more complex mantle flow patterns such as

those near subduction zones.

Regional models of lithospheric anisotropy can be constructed from the tomography of intermediate-period Rayleigh and/ or Love surface waves (*30–32*) to a nominal resolution of a few hundred kilometers. Some regional-scale studies include smaller earthquakes to increase azimuthal coverage over a smaller area; for example, from the subduction zones that surround Australia (*31*). Under continents, most studies report a transition in mantle texture within the upper mantle, possibly between shallow "fossil" lithospheric texture (likely from continental assembly) and present-day shear at the base of the plate (*30–32*).

Shear-Wave Splitting

Shear-wave birefringence, or splitting, is the most popular tool for investigating seismic anisotropy (*33–35*). In an anisotropic mantle with a horizontal symmetry axis, an upgoing shear wave will split into fast and slow polarizations at right angles to each other. Travel through the anisotropic mantle introduces a time delay δ*t* between fast- and slow-polarized *S* waves. Measurements of δ*t* and fast-polarization azimuth ϕ are sensitive to the product of layer thickness and layer anisotropy beneath an observation point, offering no direct resolution of anisotropy with depth.

Splitting data confirm many predictions of mantle flow from plate tectonics (*36*). Simple shear at the base of the North American plate has been inferred from fast polarizations in the eastern United States that align with the direction of absolute plate motion (*37*). At divergent plate boundaries, simple flow models predict fast polarization perpendicular to mid-ocean ridges, which is confirmed at the fast-spreading East Pacific Rise (*38*). At convergent margins, pure shear in the shallow mantle can explain orogen-parallel fast polarization in the Pyrenees (*39*) and New Zealand (*40*).

Where descending slabs influence mantle flow, observations are diverse. The splitting of *S* waves from slab earthquakes at various depths does not yet reveal a simple depth

dependence of mantle strain in a typical wedge (*41*). Trench-parallel flow and/or extension beneath the slab has been inferred from splitting observations in South America (*42*, *43*) and Kamchatka (*44*). Trench-normal fast polarization in the back-arc of the Kuriles and Pacific Northwest suggests an entrainment of mantle by viscous coupling to the slab (*45*, *46*). In selected Pacific subduction zones, the fast polarization aligns with the back-arc spreading direction, rather than with slab velocity (*47*). A lack of splitting is sometimes seen (*47*, *48*) and may imply a poorly developed wedge flow (*49*).

In two cases, the central Apennines of Italy (*50*, *51*) and the Lau Basin of the southwest Pacific (*52*), fast polarization near the trench rotates to trench-normal in the back-arc region. Splitting in the Apennines was estimated from teleseismic *S* waves, so that trench-parallel fast polarization near the trench may indicate mantle strain beneath or within the slab, not above it. However, in the Apennines back-arc, the P_n fast orientation is trench-parallel (*50*, *51*). Its disagreement with the splitting fast polarization is another indication of depth-dependent mantle-wedge flow.

Continental shields often exhibit fossil mantle textures, dating from rifting, collision, and accretion events as old as a billion years or more. Fast polarization aligns with the trends of Precambrian tectonic features in the Canadian shield (*53*, *54*) and with a late Proterozoic collisional zone in the Arabian Shield (*55*, *56*). In southern Africa, the fast polarization aligns consistently through both Archean and Proterozoic continental cratonic zones (*57*). Tectonically active continental regions may suffer localized lithospheric flows. For instance, fast polarization in the Snake River Plain aligns with the shearing motion of North America over the Yellowstone hot spot, but the poor coherence of splitting fast axes elsewhere in the western United States (*46*) argues for more complex regional mantle flow.

The interpretation of shear-wave splitting is more difficult when more than one anisotropic layer is present. Because each distinct anisotropic layer generates pairs of fast and slow shear waves, each layer (in theory) doubles the number of incoming waves to interpret. Because splitting times δ*t* ∼ 1 s are typical, and teleseismic core-refracted waves are typically analyzed at periods >5 s, splitting is estimated from elliptical seismic motion in the horizontal plane, not from distinct wave arrivals. The effects of multiply split waves are amalmagated into a single apparent splitting measurement, found by searching a range of δ*t* and fast-polarization azimuth ϕ values for those that best represent the elliptical motion. Such processing oversimplifies the birefringence caused by two or more layers of distinct anisotropy, but interpretation

is possible from strong variations of δ*t* and φ with the approach azimuth and incidence angle of the shear wave (*58*). Such variation was first found at observation points proximal to the San Andreas Fault in California. Fast polarization in the upper layer, perhaps most affected by the brittle deformation of the fault zone, is roughly fault-parallel, whereas fast polarization in the lower layer is roughly east-west, consistent with fast polarization farther inland beneath the Sierra Nevada foothills.

Anisotropy with a plunging symmetry axis also exhibits a variation of δ*t* and φ that can be distinguished from a multiple-layer effect (*59*). Plunging-axis effects are reported in much of Europe, with textures perhaps developed during the Variscan orogeny of the late Paleozoic (*60*), and from a sandwich of old Archean subducted slabs (*61*). Birefringence estimates in the northeastern United States are consistent with a horizontal symmetry axis in the upper layer, interpreted to be fossil lithospheric strain related to a Paleozoic delamination event (*62*), and a plunging axis in the bottom layer. The plunging axis aligns with absolute plate motion, similar to splitting in the mideastern and central United States (*37*) and thus agrees with Zhang and Karato (*6*) regarding modest simple shear textures in olivine aggregates. However, Fouch *et al.* (*37*) interpret *SKS* splitting

in terms of asthenospheric flow around a notch in the base of the North American continental lithosphere. Both interpretations are corroborated by a coincident low shear-velocity anomaly in regional-scale surface-wave tomography (*63*), but for different reasons (*64*). Many splitting observations are coherent across a local network of stations in the northeastern United States, consistent with the two-layer interpretation (*62*).

Ambiguity in shear-wave splitting is inevitable, because splitting integrates anisotropic properties along a wave's path. Ray paths of core-refracted shear waves are near parallel, without the crossing patterns that allow anomalies to be localized. Multiple layers can be invisible to sparse data sets. Numerical experiments have indicated that sparse data and popular data-averaging techniques can lead to a bias toward the fast-polarization direction of the uppermost anisotropic layer (*65, 66*), which may help explain why many splitting observations correlate with surface tectonic features.

Surface-Wave Scattering

The close connection of shear-wave birefringence parameters to regional tectonics argues that anisotropy can vary greatly, in continents at least, over short distances. The difficulty of relating anisotropy from surface-wave tomog-

raphy to broad-scale tectonics is therefore not surprising. Some surface-wave scattering effects, however, are quite sensitive to lateral gradients in anisotropy. Surface-wave scattering from Love (horizontally polarized shear) to Rayleigh (hybrid shear and compression) motion at long periods (>70 s) can be strong evidence for lateral gradients in anisotropy at 100 to 300 km depth (*67–69*). Such quasi-Love studies have illuminated localized regions of mantle strain near several plate boundaries and other geodynamic features. The seaward sides of several Pacific subduction zones (Tonga-Kermadec, Japan-Kurile, and the central Aleutians) exhibit quasi-Love observations that are consistent with strong trench-parallel flow and/or extension in the asthenosphere beneath the subducting slab (*68, 70*). There is a rough correlation between quasi-Love amplitude, back-arc spreading, and inferred trench rollback. Large quasi-Love amplitudes are observed near Tonga-Kermadec (*67, 68*), where back-arc spreading and rollback are large, and smaller amplitudes are observed at Kamchatka, where back-arc activity is ambiguous (*71*).

Quasi-Love waves are generated in the mantle beneath the Tangula-Shan mountains (Fig. 3), a convergence zone at the southern edge of the Tibetan Plateau (*72*). A mantle anisotropy model based on shear-wave splitting in Tibet (*73*) predicts this scattering
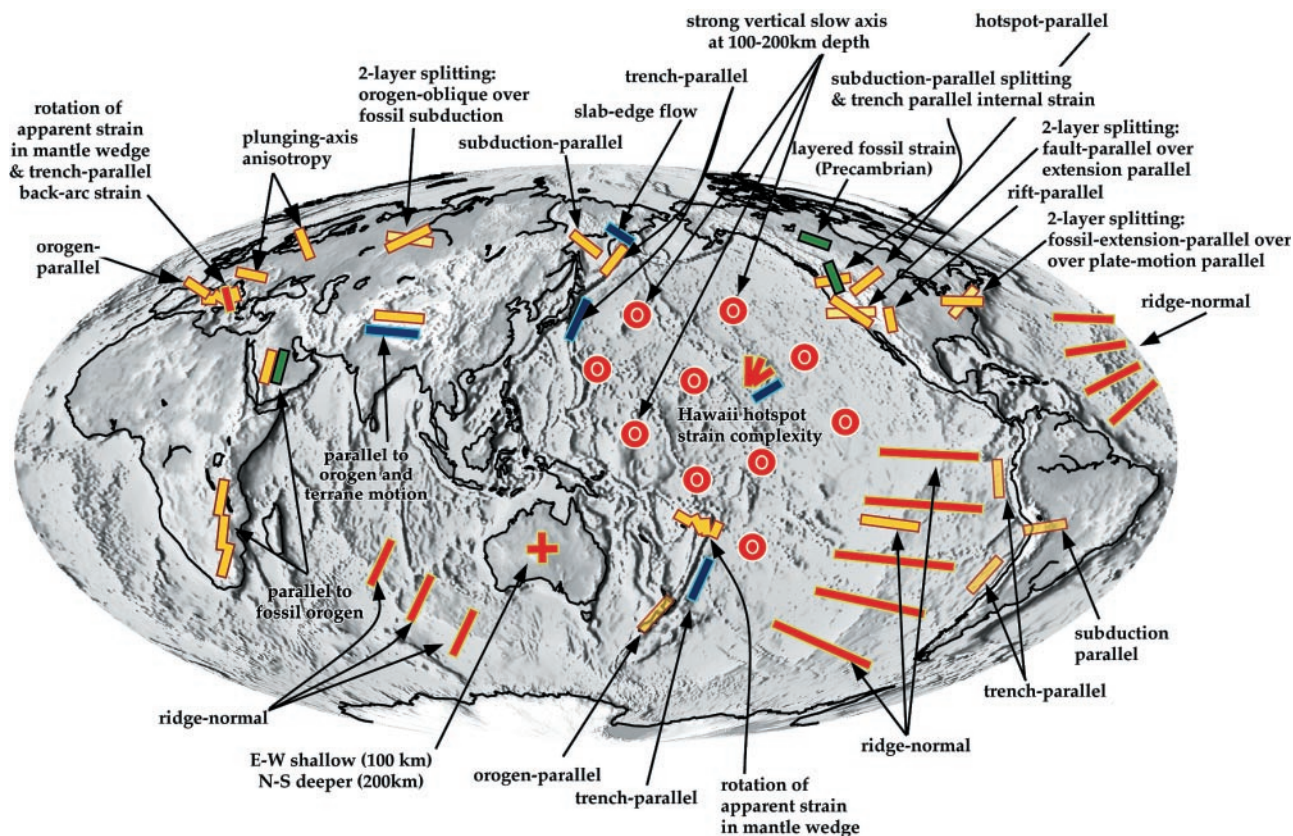
Fig. 2. Selective global compilation of seismic anisotropy results. Line segments indicate the orientation of the inferred symmetry axis, corresponding to the fast symmetry axis of mantle peridotite except where noted. Symbol length is arbtrary. Symbol color indicates the type of seismic observation: red, surface-wave and *P*ₙ tomography; yellow, shear-wave birefringence; blue, surface-wave scattering; green, *P*-to-*S* scattered waves.
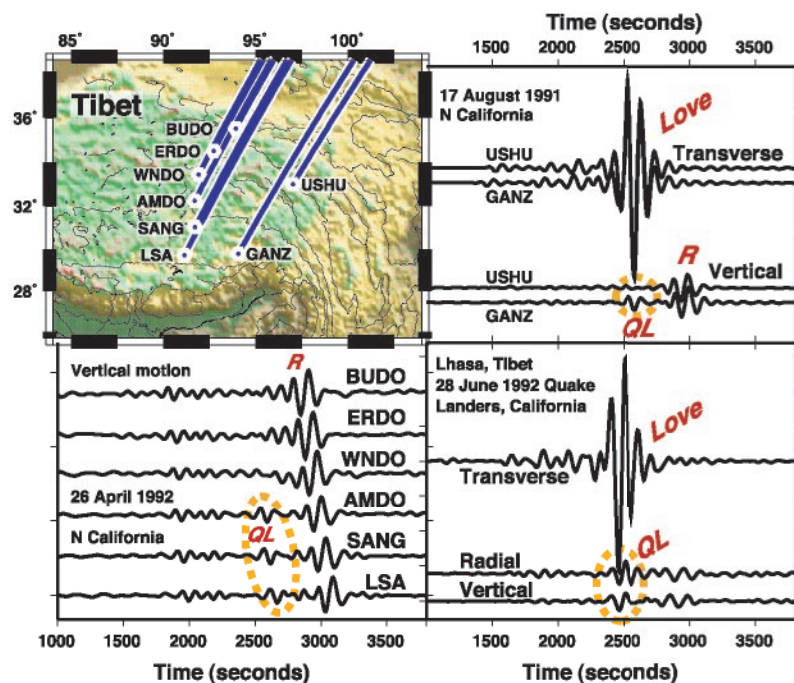
Fig. 3. Love-to-Rayleigh surface-wave scattering in the Tibetan Plateau. Portable seismological stations are marked, with propagation paths of surface waves from California earthquakes. The quasi-Love (*QL*) scattered phase was generated by the Love wave as it passed through the southern plateau, between stations USHU and GANZ to the east and between stations WNDO and AMDO in the central plateau. Seismic signals are low-passed at 100 s and rotated to radial and transverse horizontal coordinates to isolate the Love wave. The *QL* wave diagnoses a sharp lateral gradient in anisotropic properties in the southern plateau. The waveforms can be modeled with localized 4% V_S anisotropy at 100 to 300 km depth with an east-west horizontal fast symmetry axis (*72*).
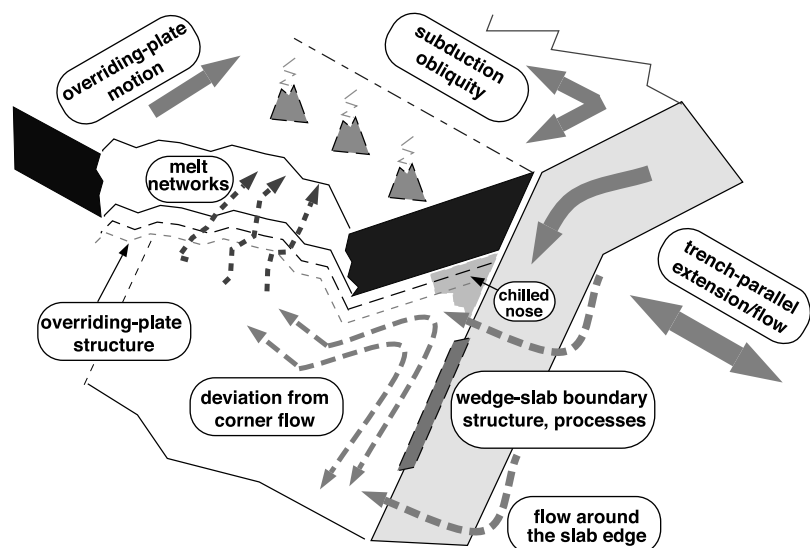

Fig. 4. Summary of processes that influence mantle anisotropy in plate tectonic subduction zones and that may be probed with seismic waves. Thick gray arrows show motions of plates and possible trench-parallel flow induced by rollback of the subducting slab. Thin dashed arrows show possible flow patterns in the mantle wedge and melt/volatile plumbing under the volcanic arc. Such processes probably produce seismic anisotropy in the mantle. The overriding plate may be thicker or thinner (resolvable with receiver functions). The degree of coupling between the plate and wedge material has a strong influence on the resulting flow pattern. Volatiles near the slab surface may control viscosity and the degree of wedge-slab coupling. Coupling of wedge material to the boundaries can potentially be deduced from the sharpness and texture of transition regions. A "chilled nose" predicted by some thermal models (*91*) may exhibit anisotropic texture and affect upper-mantle seismic wavespeed.

poorly, lending weight to the correlation between splitting and surface tectonics (*74*) and perhaps shallower (<100 km) lithospheric strain. The surface waves suggest a concentration of compressive pure shear in the mantle beneath the southern edge of the plateau, perhaps in response to the collision of the Indian subcontinent from the south (*72*).

Hot spots in the mantle may generate predictable flow patterns beneath moving lithosphere, with a bow shock gradient forward of the rising plume and a long sheared tail (*75*). Quasi-Love waves are observed at Hawaii, presumably generated by the bow shock gradient in mantle flow (*76*). Surface-wave tomography (*21*, *25*) finds a broad concentration of vertical axis anisotropy and strong variations in azimuthal anisotropy near the Hawaii hot spot, consistent with a disturbance in shallow mantle flow.

Ps Converted Waves

Compressional (*P*) waves that convert partially to shear (*S*) polarization offer the finest resolution of vertical anisotropic layering in the upper mantle. At an interface between two rock layers, anisotropy both magnifies the partial conversion of *P* to *S* motion to form a '*Ps* seismic phase and varies *Ps* amplitude with incoming wave direction to distinguish plunging from horizontal symmetry axes (*77*–*79*). The receiver function (RF) deconvolution technique retrieves *Ps* converted phases from complex *P* waves from earthquakes (*80*, *81*).

The largest P_s converted phases typically arise from the Mohorovicic discontinuity (the Moho) between crust and mantle. RF studies of stations in the Urals suture zone (*13*, *81*) and the Arabian shield (*56*) display transverse-component *Ps* motion consistent with shear zones above and below the Moho, respectively. A slow axis of symmetry is inferred in the Urals. This suggests layers of crustal or hybrid crust/mantle lithology, characterized by abundant sheet silicates in the crustal rocks, such as metapelites (*12*); the presence of fine layering (*11*); or aligned microcracks (*10*).

Ps arrivals from deeper interfaces within the continental lithosphere have been reported with behavior consistent with anisotropy. Receiver functions for the Lehmann discontinuity (~220 km) in the Slave Province of the Canadian Shield (*82*) support hypotheses that it arises from a change in mantle fabric (*83*, *84*). The Hales discontinuity (~80 km) appears as a finite (10- to 20-km) layer of strong anisotropy in both the Slave Province (*82*) and the Arabian Shield (*56*).

Ps converted phases are commonly observed from interfaces atop downgoing lithosphere in subduction zones (*85*, *86*). Data from the Cascadia subduction zone indicate an anisotropic zone with trench-parallel sym-

metry, possibly shear strain from trench-parallel migration of the overriding coastal terrane (*87*).

An Emerging Picture of Mantle Flow, Past and Present

Although seismic anisotropy is our most direct indicator of upper mantle deformation, its interpretation is far from simple. A global map of inferred anisotropic strength and orientation would not translate directly into a global map of shallow-mantle convective motions. Worse, our resolution of elastic anisotropy, on a global scale, is far from complete. Recent observational studies have highlighted small-scale anisotropic features that indicate shear localization, a potential source of bias in path-integral observables of anisotropy, such as tomographic phase delays and shear-wave birefringence. Nevertheless, the growing number of seismic techniques promises a wealth of new discoveries in the next decade.

The scope of upper mantle anisotropy studies has progressed far beyond the initial goal of mapping broad-scale convection patterns. The relationship between bulk deformation and anisotropic geometry depends on microscopic processes that are influenced by temperature, water content, and strain history—factors more numerous than can now be constrained on a global scale. In addition, scattered-wave indicators of anisotropy, such as quasi-Love waves and *Ps* converted waves, argue for short-wavelength anisotropic gradients suggestive of localized shear zones. Shear localization in the mantle and crust should not be surprising, as there are many field examples of highly deformed rock, such as mylonites (*88*) and earthquake fault zones themselves.

New interpretation approaches for elastic anisotropy are emerging. Matching seismic data with a self-consistent model of mantle flow and rock deformation is challenging, however. At mid-ocean ridges, where oceanic plates are formed, a rift-normal fast-axis orientation suggests a straightforward relationship between anisotropy and plate divergence (*23*, *25*, *29*). Although simple continuous flow models predict anisotropic texture to be frozen into young oceanic plate as it cools and thickens (*7*), more sophisticated modeling of olivine crystal aggregates suggests that anisotropic texture can be weak in the stiff plate and concentrated in the lithosphere-asthenosphere transition (*89*, *90*).

Subduction zones are another plate boundary where mantle anisotropy may help prioritize competing processes (Fig. 4). Most petrologic models of the "subduction factory" assume that shear coupling to the downgoing slab drives a two dimensional corner flow in the upper-mantle wedge above it (*91*). Observational evidence for a uniform trench-normal mantle fabric is not widespread (*44*, *47–50*, *52*); rather, there is evidence that mantle strain has strong vertical variation (*44*, *51*, *71*). Flow complexity here would strongly influence island arc volcanism and the accretion of continents, processes that remain unsolved puzzles of plate tectonic theory.

References and Notes

1. V. Babuska, M. Cara, *Seismic Anisotropy in the Earth* (Kluwer Academic, Dordrecht, Netherlands, 1991).
2. M. Kumazawa, O. L. Anderson, *J. Geophys. Res.* **74**, 5961 (1969).
3. Pyroxene crystals are similarly anisotropic but less abundant, and contribute to bulk anisotropy in mantle peridotite.
4. A. Nicolas, F. Boudier, A. M. Boulier, *Am. J. Sci.* **10**, 853 (1973).
5. N. I. Christensen, *Geophys. J. R. Astron. Soc.* **76**, 89 (1984).
6. S. Zhang, S.-I. Karato, *Nature* **375**, 774 (1995).
7. N. M. Ribe, *Geophys. J.*, **97**, 199 (1989).
8. _____, Y. Yu, *J. Geophys. Res.* **96**, 8325 (1991).
9. H. Jung, S.-I. Karato, *Science* **293**, 1460 (2001).
10. S. Crampin, *Geophys. J. R. Astron. Soc.* **76**, 135 (1984).
11. G. E. Backus, *J. Geophys. Res.* **67**, 4427 (1962).
12. J. E. Quick, S. Sinigoi, A. Mayer, *Geology* **23**, 739 (1995).
13. V. Levin, J. Park, *Geophys. Res. Lett.* **24**, 1283 (1997).
14. P. B. Kelemen, H. J. B. Dick, *J. Geophys. Res.* **100**, 423 (1995).
15. S. Zhang, S.-I. Karato, J. FitzGerald, U. H. Faul, Y. Zhou, *Tectonophysics* **316**, 133 (2000).
16. E. Kaminski, N. M. Ribe, *Earth Planet. Sci. Lett.* **189**, 253 (2001).
17. H. R. Wenk, K. Bennett, G. R. Canova, A. Molinari, *J. Geophys. Res.* **96**, 8337 (1991).
18. P. M. Shearer, J. A. Orcutt, *Geophys. J. R. Astron. Soc.* **87**, 967 (1986).
19. G. B. Morris, R. W. Raitt, G. G. Shor, *J. Geophys. Res.*, **74**, 4300 (1969).
20. T. G. Masters, P. M. Shearer, in *Global Earth Physics: A Handbook of Physical Constants* (American Geophysical Union, Washington, DC, 1995), p. 88–103.
21. G. Ekstrom, A. D. Dziewonski, *Nature* **394**, 168 (1998).
22. M. F. Smith, F. A. Dahlen, *J. Geophys. Res.* **78**, 3321 (1973).
23. J.-P. Montagner, T. Tanimoto, *J. Geophys. Res.* **96**, 20337 (1991).
24. J.-P. Montagner, *Pure Appl. Geophys.* **151**, 223 (1998).
25. G. Laske, G. Masters, *Geophys. J. Int.* **132**, 508 (1998).
26. J. J. Leveque, E. Debayle, V. Maupin, *Geophys. J. Int.* **133**, 529 (1998).
27. J. Trampert, J. H. Woodhouse, *Eur. Geophys. Soc. Newslett.* **58**, 57 (1996).
28. Y.-S. Zhang, T. Lay, *Phys. Earth Planet. Int.* **114**, 71 (1999).
29. G. Silveira, E. Stutzmann, D.-A. Griot, J.-P. Montagner, L. M. Victor, *Phys. Earth Planet. Int.* **106**, 257 (1998).
30. A. Li, D. W. Forsyth, K. M. Fischer, *Eos Trans. AGU* **80**, Fall Meeting Suppl., F730 (1999).
31. E. Debayle, B. L. N. Kennett, *Earth Planet. Sci. Lett.* **184**, 339 (2000).
32. D.-A. Griot, J.-P. Montagner, P. Tapponnier, *Geophys. Res. Lett.* **25**, 1447 (1998).
33. L. P. Vinnik, G. L. Kosarev, L. I. Makeyeva, *Dokl. Akad. Nauk SSSR* **278**, 1335 (1984).
34. P. G. Silver, W. W. Chan, *Nature* **335**, 34 (1988).
35. M. K. Savage, *Rev. Geophys.* **37**, 65 (1999).
36. P. G. Silver, *Annu. Rev. Earth Planet. Sci.* **24**, 385 (1996).
37. M. J. Fouch, K. M. Fischer, E. M. Parmentier, M. E. Wysession, T. J. Clarke, *J. Geophys. Res.* **105**, 6255 (2000).
38. C. J. Wolfe, S. C. Solomon, *Science* **280**, 1230 (1998).
39. G. Barruol et al., *J. Geophys. Res.* **103**, 30039 (1998).
40. P. Molnar et al., *Science* **286**, 516 (1999).
41. M. J. Fouch, K. M. Fischer, *J. Geophys. Res.* **101**, 15987 (1996).
42. R. M. Russo, P. G. Silver, *Science* **263**, 1105 (1994).
43. J. Polet et al., *J. Geophys. Res.* **105**, 6287 (2000).
44. V. Peyton et al., *Geophys. Res. Lett.* **28**, 379 (2001).
45. L. Su, J. Park, *Phys. Earth Planet. Int.* **86**, 263 (1994).
46. D. L. Schutt, E. D. Humphreys, *Geology* **29**, 291 (2001).
47. K. M. Fischer, M. Fouch, D. Wiens, M. Boettcher, *Pure Appl. Geophys.* **151**, 463 (1998).
48. S. Weimer, G. Tytgat, M. Wyss, U. Duenkel, *Bull. Seism. Soc. Am.* **89**, 1313 (1999).
49. J. Buttles, P. Olson, *Earth Planet. Sci. Lett.* **164**, 245 (1998).
50. L. Margheriti, C. Nostro, M. Cocco, A. Amato, *Geophys. Res. Lett.* **23**, 2721 (1996).
51. A. Amato et al., *Pure Appl. Geophys.* **151**, 479 (1998).
52. G. P. Smith et al., *Science* **292**, 713 (2001).
53. P. G. Silver, S. Kaneshima, *Geophys. Res. Lett.* **20**, 1127 (1993).
54. S. Rondenay, M. G. Bostock, T. M. Hearn, D. J. White, R. M. Ellis, *J. Geophys. Res.* **105**, 13735 (2000).
55. C. J. Wolfe, F. L. Vernon III, A. Al-Amri, *Geophys. Res. Lett.* **26**, 779 (1999).
56. V. Levin, J. Park, *Tectonophysics* **323**, 131, (2000).
57. P. G. Silver, S. S. Gao, K. H. Liu, Kaapvaal Seismic Group, *Geophys. Res. Lett.* **28**, 2493 (2001).
58. P. G. Silver, M. K. Savage, *Geophys. J. Int.* **119**, 949 (1994).
59. V. Babuska, J. Plomerova, J. Sileny, *Phys. Earth Planet. Int.* **78**, 167 (1993).
60. J. Plomerova et al., *Tectonophysics* **332**, 1 (2001).
61. J. Plomerova et al., *Studia Geophys. Geod.* **44**, 195 (2000).
62. V. Levin, W. Menke, J. Park, *J. Geophys. Res.* **105**, 19029 (2000).
63. S. van der Lee, G. Nolet, *J. Geophys. Res.* **102**, 22815 (1997).
64. Levin et al. (*62*) cite low V_S as evidence of an iron-rich asthenosphere that replaced a foundered lithospheric root, subsequently cooling and dehydrating to join the lithosphere. Fouch et al. (*37*) cite low V_S as evidence for a patch of thinned lithosphere, beneath which asthenospheric flow must deflect.
65. G. Rumpker, P. G. Silver, *Geophys. J. Int.* **135**, 790 (1998).
66. R. L. Saltzer, J. B. Gaherty, T. H. Jordan, *Geophys. J. Int.* **141**, 374 (2000).
67. J. Park, Y. Yu, *Science* **261**, 1159 (1993).
68. Y. Yu, J. Park, *J. Geophys. Res.* **99**, 15399 (1994).
69. H. Oda, S. Onishi, *Geophys. J. Int.* **144**, 247 (2001).
70. R. Kobayashi, I. Nakanishi, *Geophys. Res. Lett.* **25**, 1067 (1998).
71. J. Park et al., in *Plate Boundary Zones*, S. Stein, Ed. (American Geophysical Union, Washington, DC), in press.
72. Y. Yu, J. Park, F. Wu, *Phys. Earth Planet. Int.* **87**, 231 (1995).
73. D. E. McNamara, T. J. Owens, P. G. Silver, F. T. Wu, *J. Geophys. Res.* **99**, 13655 (1994).
74. W. E. Holt, *Geology* **28**, 67 (2000).
75. N. M. Ribe, U. R. Christensen, *J. Geophys. Res.* **99**, 669 (1994).
76. V. Levin, J. Park, *J. Geophys. Res.* **103**, 24321 (1998).
77. J. F. Cassidy, *Bull. Seism. Soc. Am.* **82**, 1453 (1992).
78. V. Levin, J. Park, *Pure Appl. Geophys.* **151**, 669 (1998).
79. M. K. Savage, *J. Geophys. Res.* **103**, 15069 (1998).
80. C. J. Ammon, *Bull. Seism. Soc. Am.* **81**, 2504 (1991).
81. J. Park, V. Levin, *Bull. Seism. Soc. Am.* **90**, 1507 (2000).
82. M. G. Bostock, *J. Geophys. Res.* **103**, 21183 (1998).
83. S.-I. Karato, *Geophys. Res. Lett.* **19**, 2255 (1992).
84. J. B. Gaherty, T. H. Jordan, *Science* **268**, 1468 (1995).
85. G. L. Kosarev et al., *Science* **283**, 1306 (1999).
86. ANCORP Working Group, *Nature* **397**, 341 (1999).
87. H. Yuan, J. Park V. Levin, *J. Geophys. Res.*, in press.
88. S. Siegesmund, M. Fritzsche, G. Braun, in *Continental Lithosphere: Deep Seismic Reflections*, R. Meissner et al., Eds. (American Geophysical Union, Washington, DC, 1991), pp. 291–298.
89. A. Tommasi, *Earth Planet. Sci. Lett.* **160**, 1 (1998).
90. D. K. Blackman et al., *Geophys. J. Int.* **127**, 415 (1996).
91. S. M. Peacock, K. Wang, *Science* **286**, 937 (1999).
92. Supported by NSF grant EAR-9805206. Discussion with S.-I. Karato helped to clarify important points.